Coastal Engineering 188 (2024) 104451

Contents lists available at ScienceDirect

Coastal Engineering

journal homepage: www.elsevier.com/locate/coastaleng

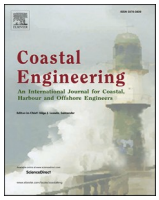

Satellite observations of storm erosion and recovery of the Ebro Delta coastline, NE Spain

C. Cabezas-Rabadán [a,b,*], J.E. Pardo-Pascual [a], J. Palomar-Vázquez [a], A. Roch-Talens [a], J. Guillén [c]

[a] Geo-Environmental Cartography and Remote Sensing Group (CGAT-UPV), Department of Cartographic Engineering, Geodesy and Photogrammetry, Universitat Politècnica de València, Camí de Vera s/n, València, Spain
[b] Univ. Bordeaux, CNRS, Bordeaux INP, EPOC, UMR 5805, F-33600, Pessac, France
[c] Institute of Marine Sciences (CSIC), Passeig Maritim de la Barceloneta 37-49, Barcelona, 08003, Spain

ARTICLE INFO

Keywords:
Subpixel shoreline extraction
Coastal storm monitoring
Beach morphological characterisation
SAET
Sentinel-2
Landsat
Erosion and recovery

ABSTRACT

Storms and extremely energetic events may significantly impact the form and structure of beaches, and so cause erosive processes and coastal damages. Efficient management actions require an up-to-date and accurate knowledge of beach morphological changes, with the shoreline position being a good indicator of such changes. This work proposes the use of the open-source Shoreline Analysis and Extraction Tool (SAET) software for the definition of satellite-derived shorelines (SDSs) from L8 and Sentinel-2 imagery to reveal the shoreline position changes at the beaches of the Ebro Delta, NE Spain. Spatial-temporal models (STMs) of shoreline changes enable a characterisation of how the beaches responded to the storms of 2020. In conjunction with wave data, STMs enable an analysis of the erosive response to storm events, as well as a monitoring of subsequent beach recovery in the short and medium term (<1 year). Results show how Storm Gloria (January 2020, Hs max = 7.62 m) acted as a disruptive event and shifting point in the shoreline trend. As a response to that storm, major erosive processes occurred along the delta that caused an average shoreline retreat of 47 m. A progressive recovery during the spring and summer was mainly associated with periods of low wave energy. Nevertheless, by the end of the year a complete recovery had been achieved for about half of the coast, while the other half showed an average erosion of more than 10 m when compared to the pre-storm situation. Both the erosive and the recovery processes took place unevenly on different sections of the coast, probably dependent on factors such as the orientation of the beach and the pattern of longitudinal sediment transport along the coast.

1. Introduction

Beaches are spaces that show a high dynamism as a response to the oceanographic conditions to which they are subjected (Ciavola and Coco, 2017). Energetic episodes may produce large cross-shore and longshore sediment transport (Burvingt et al., 2017) that changes the form and structure of beaches (Anfuso et al., 2020) as well as the sediment texture (Prodger et al., 2016). It is to be expected that the response to storms varies along the coast according to the beach characteristics (Pardo-Pascual et al., 2014) such as the exposure to the incident waves (Burvingt et al., 2017). Extreme storms may drastically change the configuration of the coastline by redistributing and mobilising the sediment, sometimes leading to the landward migration of the shore (Castelle and Harley, 2020). When the response is not homogeneous, certain sections may exhibit significantly higher rates of erosion than adjacent areas, constituting hotspots that may or may not reverse rapidly (List et al., 2006).

Recovery may occur after the energetic episode (Castelle and Harley, 2020; Morton et al., 1994; Sénéchal et al., 2015) with different intensity greatly depending on the sediment availability and hydrodynamic conditions (Lee et al., 1998). The rebuilding of the subaerial beach would depend on the combination of mechanisms such as sediment transport from the nearshore to the beach, swash and aeolian processes (Phillips et al., 2019; Hu et al., 2023). In equilibrium beaches, this

* Corresponding author. Geo-Environmental Cartography and Remote Sensing Group (CGAT-UPV), Department of Cartographic Engineering, Geodesy and Photogrammetry, Universitat Politècnica de València, Camí de Vera s/n, València, Spain.
E-mail addresses: carcara4@upv.es (C. Cabezas-Rabadán), jepardo@cgf.upv.es (J.E. Pardo-Pascual), jpalomav@upvnet.upv.es (J. Palomar-Vázquez), aurocta@alumni.upv.es (A. Roch-Talens), jorge@icm.csic.es (J. Guillén).

https://doi.org/10.1016/j.coastaleng.2023.104451
Received 22 June 2023; Received in revised form 30 November 2023; Accepted 27 December 2023
Available online 30 December 2023

process leads to a morphological configuration like that before the storm. In this case, it would be an oscillatory process without a strong effect superimposed on long-term evolutionary dynamics. In contrast, when these changes cannot be compensated in the short term, they may constitute breakpoints in the morphological evolution of the affected beaches (Sénéchal et al., 2017) therefore impeding the complete recovery of the beach even over the course of a year (Castelle et al., 2015). As there are still gaps in our knowledge about how beach responses to storms are modulated over space and time, it is worthwhile analysing the impact and the short- (days) and mid-term (months) recovery processes following large storms on large coastal segments with differing conditions.

On Mediterranean coasts, the maintenance of the physical characteristics of the beaches constitutes a major concern for coastal managers (Ariza et al., 2008). The geomorphological changes that occur as a response to storm episodes may jeopardize the physical integrity and maintenance of the functions of the beaches (Cabezas-Rabadán et al., 2019a). Because of global warming (IPCC et al., 2021), the higher frequency of extreme weather events and the magnitude of storms together with sea level rise may be increasing and causing accelerated shoreline erosion (Schlacher et al., 2008; Slott et al., 2006). In the western Mediterranean, storm events of remarkably high magnitude have been registered in recent years as well as increasing wave heights (Amarouche et al., 2021; Pardo-Pascual et al., 2022a). Among them, Storm Gloria is the most outstanding episode in the historical series due to its oceanographic conditions (De Alfonso et al., 2021; Pérez-Gómez et al., 2021) and the resulting erosive processes and coastal damage (Berdalet et al., 2020; Flor-Tey, 2021; Guillén, 2020; Pintó et al., 2020; Pardo-Pascual et al., 2022b; Sancho-García et al., 2021; Angelats et al., 2022).

As a response to coastal erosion, emergency actions are often carried out without the required planning or vision (Jiménez et al., 2012). It is often difficult or impossible to obtain the up-to-date and homogeneous information on the shape and structure of beaches that efficient coastal management requires. The monitoring of large segments can be achieved using various techniques. This is the case of three-dimensional monitoring through topo-bathymetric profiling campaigns or successive surveys of three-dimensional models (using LIDAR techniques). However, this type of analysis is costly and difficult to apply over large areas during long periods of time. The recent possibility of accessing optical satellite images from the Landsat and Sentinel-2 constellations at no cost has led to various approaches for efficiently mapping beaches. As the shoreline position constitutes a useful indicator of the state of beaches (Boak and Turner, 2005) and a good indicator for characterising recovery processes (Phillips et al., 2017), various approaches for the identification of shoreline positions (Satellite-Derived Shorelines, SDSs) and their changes over time have been proposed. Some algorithms and methodological solutions aim to define SDSs in a semiautomatic way with subpixel accuracy, therefore overcoming the limitations imposed by the coarse pixel size in these images (e.g., Bishop-Taylor et al., 2019; Hagenaars et al., 2018; Liu et al., 2017; Pardo-Pascual et al., 2012). Sustained by the advantages offered by these algorithms, tools such as CASSIE (Almeida et al., 2021), CoastSat (Vos et al., 2019), or SHOREX (Cabezas-Rabadán et al., 2021; Sánchez-García et al., 2020) have emerged for efficiently deriving SDSs by integrating all the required processes from downloading to the final shoreline definition (see benchmark comparison in Vos et al., 2023). These tools suffer limitations in their application for large areas or time series due to the need for user intervention or the computational limitations of working on a regional scale. The open-source toolkit SAET (Shoreline Analysis and Extraction Tool; Palomar-Vázquez et al., 2023) was recently created to automatically define and monitor shoreline positions using imagery from the ESA Copernicus program and the Copernicus Contributing Missions. Based on the SHOREX tool, SAET has been developed with the aim of offering a greater autonomy and robustness in SDS extraction than previous tools. This new tool focuses on monitoring shoreline changes when storms occur, showing an average error that ranges between 2.62 m and 8.67 m (RMSE) according to differing assessments in microtidal Mediterranean beaches (Palomar-Vázquez et al., 2023; Pardo-Pascual et al., 2023). The possibility of obtaining large packages of SDSs covering long coastal segments raises challenges for its exploitation. The spatial-temporal models (STMs) of beach changes (Cabezas-Rabadán et al., 2019b) appear as a solution to characterize the beach state when punctual events as storms affect large coastal segments, and so facilitate an analysis of temporal and geographic changes at differing scales.

The aim of this work is to demonstrate the utility of the SDSs automatically extracted using SAET in combination with STMs for studying morphological changes of the sandy beaches of the Ebro Delta as a response to coastal storms. The definition of shoreline positions over the course of a year aims to quantify the erosive response to storms and monitor their subsequent recovery.

2. Study area

The Ebro Delta (NW Mediterranean) is composed of almost 50 km of gently sloping sandy beaches (Fig. 1). The delta presents an emerged area about 350 km^2, being the two spits, which partially close the two adjacent lagoons, the main morphological features (Jiménez and Sánchez-Arcilla, 1993; Rodríguez-Santalla and Somoza, 2019). The land and dune heights behind the coast does not exceed the 5–6 m elevation (Aranda et al., 2022) and it has been highly exploited with extensive rice farming. It is a microtidal coast (tidal range about 0.2 m) with a low-energy wave regime (mean significant height of about 0.7 m and mean peak period of less than 5 s), although large waves (Hs $>$ 5 m) can be recorded during storms. The largest waves come from the first quadrant, mainly from the ENE, and to a lesser extent, from the NE. The wave pattern in combination with the deltaic morphology leads to a net longshore sediment transport towards the north (south) in the northern (southern) hemidelta (Jiménez and Sánchez-Arcilla, 1993). The Ebro Delta is a highly dynamic wave-dominated coast, largely conditioned by the reduction of sediment discharge from the Ebro River since the beginning of the 1960s (Jiménez and Sánchez-Arcilla, 1993; Rodríguez-Santalla and Somoza, 2019). This has caused strong negative rates, especially remarkable in the central lobe of the delta and the surroundings of the former river mouth favoured by the change of position of the mouth of the river (Aranda et al., 2022; Jiménez et al., 1997). Under the coexistence of eastern wave storms and surged water levels storm impacts occur along the coast (Jiménez et al., 1997). This leads to pulsating erosion behaviour as well as beach and barrier breaching and flooding events, being certain sections as Marquesa Beach, Buda Island, and Trabucador Beach remarkably vulnerable (Jiménez et al., 2012).

Several events with high waves occurred along 2020 in the NW Mediterranean (Fig. 2). The energetic events potentially affecting the Ebro Delta were identified and their magnitudes were characterised according to the wave power as proposed by Splinter et al. (2014). Among them (Table 1), Storm Gloria was by far the most energetic event, affecting the Spanish Mediterranean coast between 19 and 22 January 2020. The storm peaked on 22 of January (Hs max = 7.62 m) and heavily affected the whole of eastern Spain. This storm was a remarkably disruptive event considering its unusually large size and impact along the Western Mediterranean (Amores et al., 2020; Berdalet et al., 2020; De Alfonso et al., 2021). Evidence of the exceptional nature of Storm Gloria is provided by the change in the recurrence period of the Hs max at the Tarragona buoy, which was previously estimated to be 414 years and after the occurrence of the storm is estimated to be 48 years (de Alfonso et al., 2021). This extreme storm (which combined waves and extreme rainfall) flooded most of the Ebro delta plain, causing erosion and overwashing of the emerged beach in many deltaic areas (Berdalet et al., 2020; Flor-Tey, 2021; Pintó et al., 2020; Sancho-García et al., 2021). The emergency response to these impacts consisted of sand dumping in the most affected areas, but it became clear that more comprehensive measures were needed because of the huge

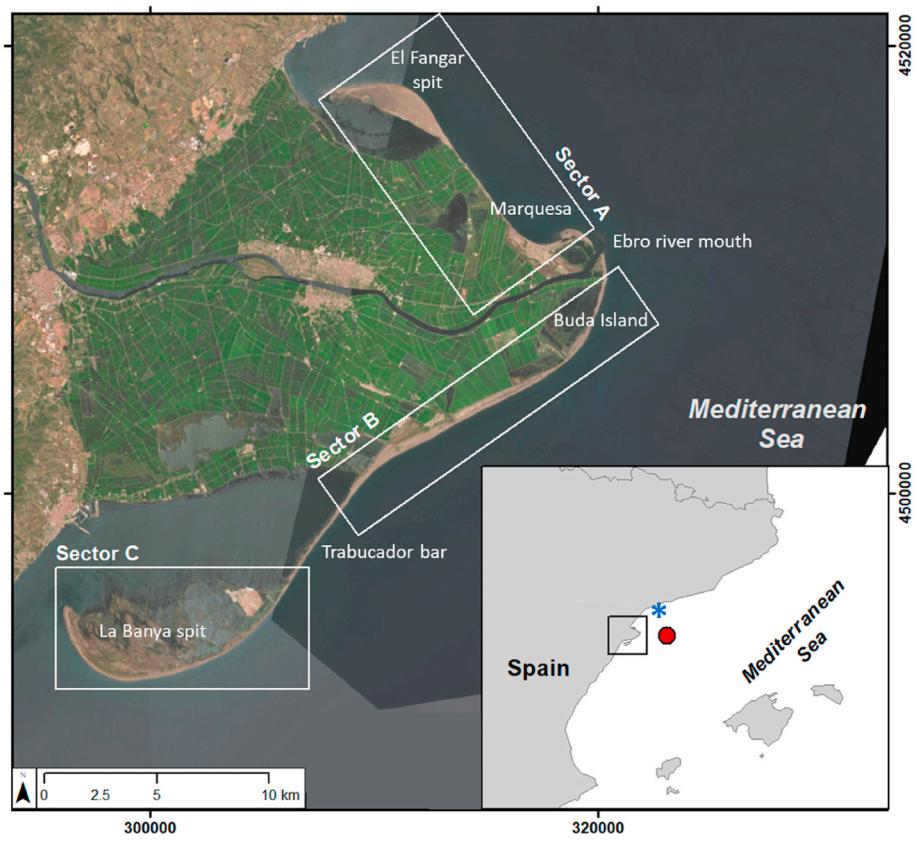

Fig. 1. Location map of the study area in Ebro Delta (NE Spain, W Mediterranean) divided in three sectors for providing greater detail in the analysis. Deployed by the Spanish port authorities, the red point and the blue asterisk indicate the buoy and the tidal gauge for retrieving wave and sea level data. Background image Sentinel-2 products © CCME (2020), provided under Copernicus by the European Union and ESA, all rights reserved. Coord. system: ETRS89 UTM31N.

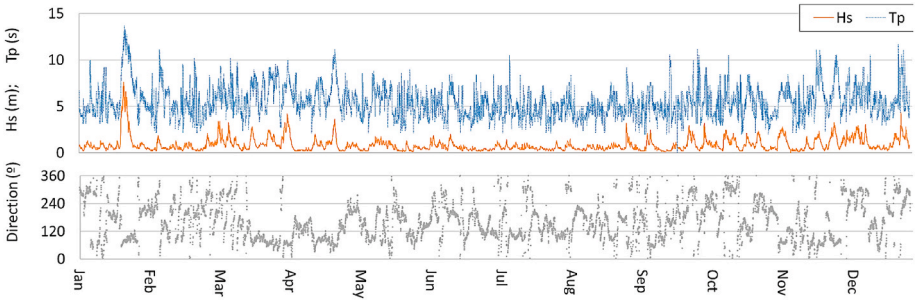

Fig. 2. Wave data (Hs, Tp and direction) along 2020 obtained from the Tarragona Buoy (see Fig. 1) from Puertos del Estado (https://www.puertos.es/).

changes caused by the storm.

The present study focused on 44.3 km of coastline composed by sandy beaches. To analyse the results, the study area was divided into three sectors (see Fig. 1). Sector A is the northernmost section (facing NW-SE) and covers 13.49 km from the current river mouth to the end of the Fangar spit. Sector B is facing NE-SW and includes the central section of the delta, covers 17.34 km between the former river mouth and the Trabucador bar. Sector C is crescent-shaped section that covers the southernmost 13.44 km of the delta between the Trabucador bar and the end of La Banya spit.

To maintain homogeneity, the areas at the mouth of the river and the Trabucador bar were not considered in the analysis. The deposition of sediment creates sand banks on the river mouth (Jiménez and Sánchez-Arcilla, 1993) close enough to the surface so they can be detected only intermittently. Regarding the Trabucador bar, it is an extremely narrow (100–200 m width) and low (about 1.5 m above mean sea level) coastal unit (Sánchez-Arcilla and Jiménez, 1994) usually overwashed and submerged several times per year when storm episodes occur (Jiménez and Sánchez-Arcilla, 1993) so its characterization requires specific analysis procedures.

3. Methodology

The positions of the shoreline during 2020 were extracted from optical satellite images using the SAET tool to generate STMs of the beach changes (Fig. 3). The position of the shoreline was horizontally corrected according to the oceanographic characteristics at the time of acquiring the satellite images. The resulting STMs were employed for analysing the beach response to the coastal storms that occurred during the year.

3.1. Definition of SDSs using SAET

The work was based on the shoreline positions derived from the

Table 1
Main storm events during 2020. They were identified when the significant wave height (Hs) was higher than 2.5 m, and it was considered as a single storm when Hs < 2.5 m for less than 12 h. Wave power was calculated as $\Sigma P = \int_o^N \frac{\rho g^2}{64\pi} Hs^2\, Tp\, \Delta t$ being ρ the sea water density, g the gravitational acceleration, Hs the deepwater significant wave height, Tp the peak wave period, Δt the measurements time step, and N the total duration of the storm. Storm Gloria is highlighted in bold. Events with direction from the coast (mainly caused by NW winds) were not consider as their impact on the Ebro Delta is negligible.

Onset of the storm (dd/mm/yy)	Mean Hs (m)	Max Hs (m)	Duration (h)	Tp (s)	Wave direct. (°N)	Wave power (kW/m^{3}s)
19/01/2020	3.99	7.62	92	11.91	82	**9493**
16/03/2020	2.58	2.81	10	8.2	68	209
31/03/2020	3	4.22	53	9.96	65	1962
22/04/2020	2.77	3.63	22	11.13	58	1022
29/08/2020	2.76	3.16	6	9.18	64	170
02/10/2020	2.91	3.16	6	8.4	225	222
05/11/2020	2.51	2.81	4	7.23	67	40
27/11/2020	2.52	2.7	2	6.64	75	22
28/11/2020	2.69	3.28	16	10.55	63	492
27/12/2020	2.78	4.34	18	10.55	227	789

optical satellite images (of equivalent pixel size) acquired by the Sentinel-2 (sensor MSI) and Landsat 8 (OLI) satellites. The images are available free of charge from the Copernicus Open Access Hub (https://dataspace.copernicus.eu/) and the Earth Explorer of the U.S. Geological Survey (USGS) (https://earthexplorer.usgs.gov/) respectively. The selection and downloading of images, as well as their pre-processing steps and the extraction of SDSs, were carried out using the SAET tool (Palomar-Vázquez et al., 2023). The selection of suitable satellite images was based on their spatial coverage and date of acquisition. The whole study site appeared covered by a single Landsat scene (198/032) and by two Sentinel-2 tiles (31TCF, 31TBE). For this scene and these tiles, all the available images during the year 2020 (that is before and after Storm Gloria) were selected. Subsequently, as described by Palomar-Vázquez et al. (2023), SAET's workflow followed four main phases: downloading of the images; creation of water indices; removal of areas affected by clouds and coastal segments that are not beaches; and finally, shoreline extraction at subpixel level. The process led to the definition of 93 shorelines (10 derived from Landsat 8, and 83 from S2). These SDSs were defined as the water/land intersection at the acquisition time of each image, and they were constituted by points located every 5 m (S2 imagery) and 7.5 m (L8). Previous assessments of the SDSs showed an estimated subpixel accuracy ranging 2.62 m–3.79 m for the beach of Valencia (W Mediterranean, Palomar-Vázquez et al., 2023) up to 8.67 m RMSE for the Ebro Delta beaches in a single test with post storm conditions (Pardo-Pascual et al., 2023).

3.2. Spatial-temporal models characterising beach changes

From the SDSs and following the methodology described by Cabezas-Rabadán et al. (2019b) a spatial-temporal model of the shoreline changes was obtained for the whole Ebro Delta (Fig. 3). A baseline divided in 60 m segments was defined, and the distance to the points defining each SDSs was measured (see Fig. 3B). For each segment the average distance for each date was calculated. Taking as a reference the

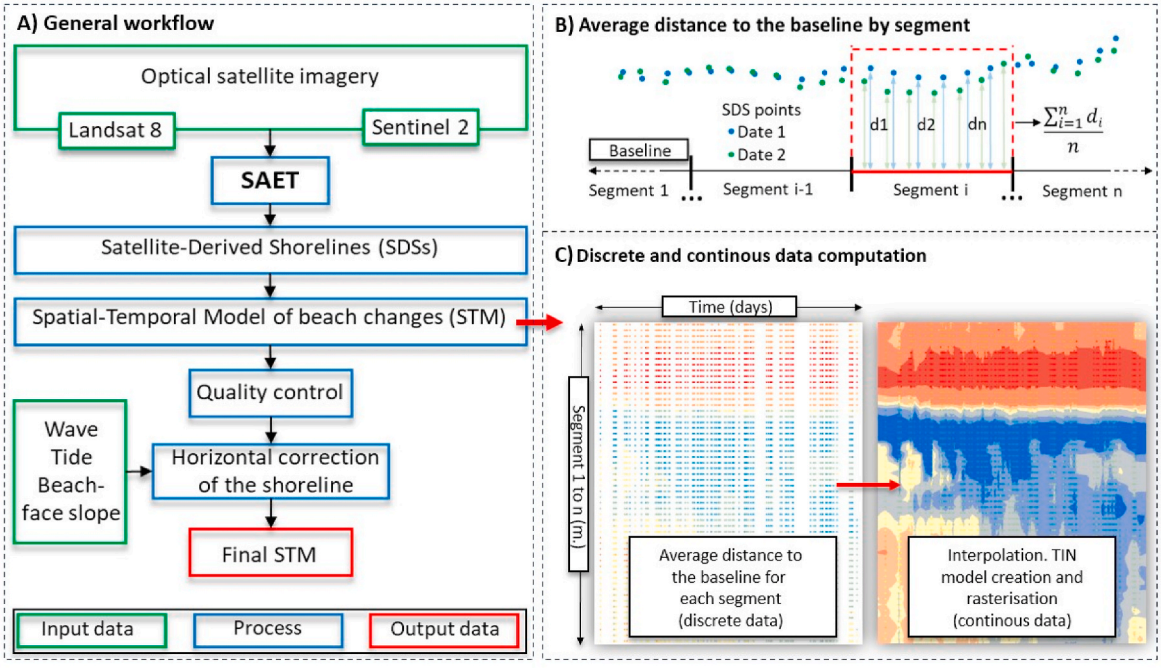

Fig. 3. A) Workflow for obtaining the corrected spatial-temporal model of the shoreline changes from satellite images and with the help of oceanographic and morphological data. B) Measurements of the distance between the points composing the SDSs and the reference baseline, and definition of the average distance for each date and baseline segment. C) Organisation of the measurements along time and space, and interpolation to transform the discrete information into continuous spatial-temporal models.

average shoreline position in January 2020 before Storm Gloria the shoreline changes were calculated, and the measurements were organized in space and time. To overcome the unequal distribution of records and to have homogeneously available data throughout all the site and the period analysed those measurements were used to deduce a continuum of values for the instants and locations without real measurement by applying a TIN interpolation – which was subsequently rasterized to generate the spatial-temporal model (see Fig. 3C). The STM consists of a Hovmöller-style diagram with the values of the shoreline changes organized in cells for time and space (60 m/day cells). This enabled overcoming the unequal distribution of records and made data homogeneously available for the whole of the study site and study period. At this point, it was verified that the observed changes were consistent with the nature of the phenomena, and the incoherent SDS positions were identified and eliminated. Subsequently, and as described in the following section, the horizontal correction of the shoreline position is carried out according to tide and wave conditions. The analysis of the resulting STM allowed the derivation of temporal profile plots of the shoreline changes broken down into three sectors (A, B, C, see Fig. 1). The profiles enabled the identification of the responses to storm events and the quantification of recovery rates for the different parts of the delta.

3.3. Tide and wave condition correction

Every image was acquired with a different sea level and wave conditions and so a correction was applied to the obtained shorelines to provide a more realistic representation of the beach changes. To do so, each shoreline was shifted to a common reference elevation. Sea level data (tidal level + storm surge) were retrieved from a tidal gauge in Tarragona Harbour, while offshore wave conditions coincident with the satellite imagery acquisition were obtained from the Tarragona buoy (see Fig. 2). Based on previous topographic data (Guillén and Palanques, 1993) the beach slope (tg β) ranged from 0.02 to 0.05 for the delta, although it was flatter at the tail of both spits (tg β = 0.008) and at the river mouth (tg β = 0.018). A mean beach slope in the surveyed areas of 0.023 was used as a reasonable approximation to estimates of shoreline location. Two corrections were applied to the position of the shoreline: a) considering the difference between the sea level measured by the tidal gauge at the time of the image with respect to the mean sea level position during the study period; and b) the wave setup, calculated according to the equation of Stockdon et al. (2006) from the wave data measured by the Tarragona buoy. The elevation of the water was calculated for the instant each SDS was acquired. Considering those elevation values together with the beach-face slope, the position of the shoreline was shifted horizontally, allowing to obtain the final STM homogenised for a similar elevation for the entire study period.

4. Results

4.1. Shoreline changes of the Ebro Delta beaches following extreme storm events

As a response to Storm Gloria, which registered its peak during the second half of January (Hs max = 7.62 m, wave power = 9493 kW/m^{3}s), important erosive processes took place along the Ebro Delta (Fig. 4). The event produced an average shoreline retreat of 47 m immediately after the storm. There were significant variations in the shoreline changes in different parts of the Ebro Delta, and in some locations the retreat exceeded 100 m. When analysing the various sectors, it can be clearly seen how sector B showed the largest landward shoreline movement (average retreat more than 60 m), followed by sector A (42 m), and sector C (24 m).

Apart from Storm Gloria, other storms registered during 2020 (see Table 1) also caused shoreline retreats. This is the case of the 16 March (wave power = 209 kW/m^{3}s) that caused an average retreat of 4.63 m although, surprisingly, it did not affect sector A. Similarly, the 27 December (wave power = 789 kW/m^{3}s) caused a significant retreat (average of 7.35 m). In turn, the storms in end of March and April (Hs max = 4.22 m the 31 March and 3.63 m the 22 April) did not appear to cause sustained erosion, although a detailed analysis is impeded by the lack of available SDSs in the dates immediately following.

The STMs show in higher detail the shoreline position changes that occurred during 2020 at the three analysed sectors (A, B, C, Figs. 5–7 respectively). Using analytical units of 60 m/day the STMs show the retreats (red-orange-yellow colours), areas of stability (changes between −5 and +5m are shown in grey), and the accretion processes (cyan blue). The average shoreline position during the first part of January, i.

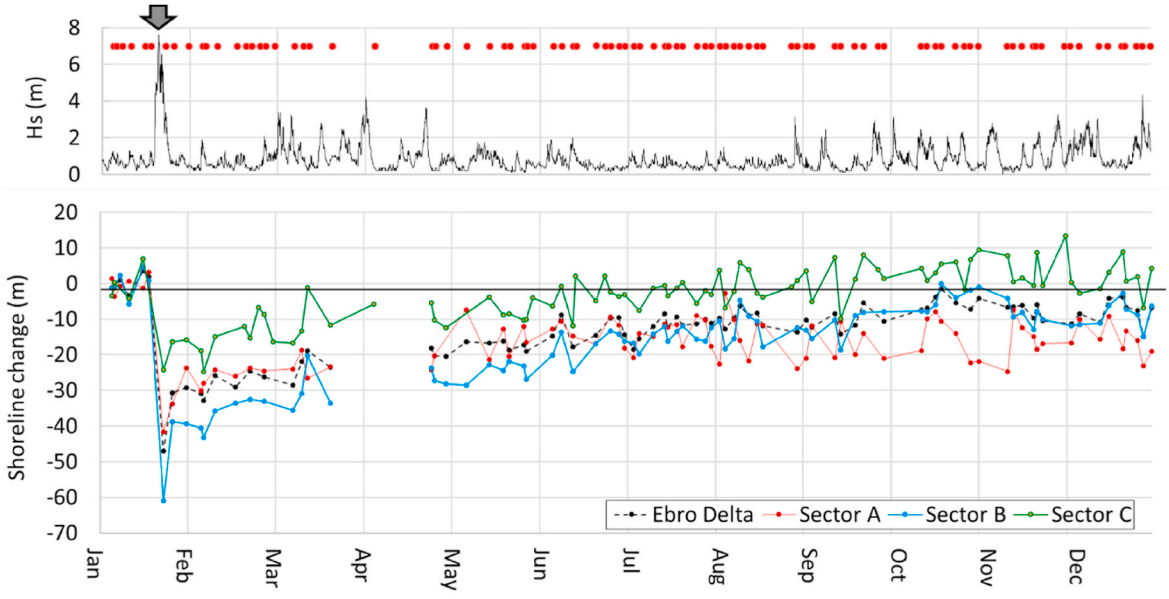

Fig. 4. Average shoreline changes along the Ebro Delta (black dashed line) and for sectors A (red line), B (blue), and C (green) taking as a reference the average position before Storm Gloria (early January). Changes are not shown between the 21 March and the 24 April due to the lack of satellite-derived shorelines in sectors A and B. At the top, significant wave height data are shown (Storm Gloria appears marked by an arrow) together with the shorelines extracted from satellite imagery for 2020.

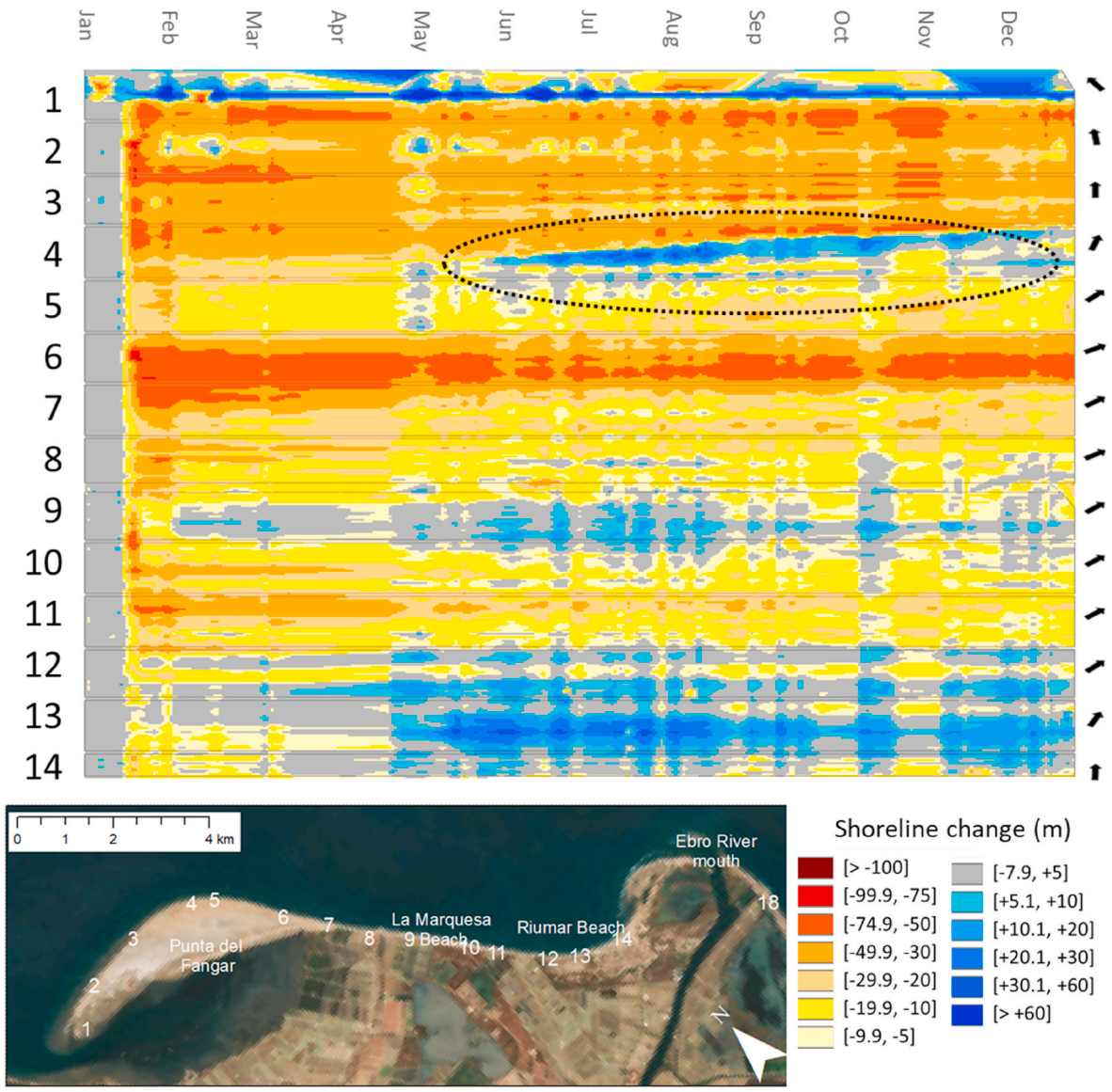

Fig. 5. Shoreline position changes at sector A covering the northernmost 14 km of the study area. The locations are presented in the image at the bottom, while arrows on the right column show the direction of a cross-shore profile towards the sea. The dashed line highlights the section showing an apparent sand wave movement as described in Fig. 9.

e., before Storm Gloria, was taken as a reference value. The wave data registered shows long periods of calm conditions, as well as several stormy periods associated with generalised changes in the shoreline position.

Punctual but strong recovery processes appeared in specific segments. This is the case of the northern and southern ends of the study area – such as the dynamic extremes of the El Fangar (km 1, sector A) and La Banya (km 51, sector C) sandspits. Associated to high dynamism, it is possible to identify a sandwave at the km 4, sector A (Fig. 8). During the second half of the year a seaward movement of the shoreline position appeared progressively towards the northwest, apparently caused by the migration of the attachment point of a longshore bar to the shoreline.

4.2. Erosive hotspots following Storm Gloria

Among the beach segments suffering the largest shoreline retreat, three zones may be highlighted due to the magnitude of the erosion as a response to Storm Gloria (Fig. 9). This is the case of (a) La Marquesa Beach, (b) Buda Island and (c) the northern extreme of Trabucador bar. Located in the central part of northern hemidelta (sector A, segments 9–11 in Fig. 5) NE-facing, La Marquesa experienced a landward movement about 50 m, with some segments exceeding the 75 m (Fig. 9, a). The greatest shoreline retreat following Gloria occurred in Buda Island the northern part of sector B (segments 18–20 in Fig. 6) facing ESE. The shoreline retreat exceeded the 100 m affecting more than 1 km of coastline alongshore, even causing the breaching of the bar (Fig. 9b). The third zone with the highest shoreline erosion corresponds to the northern edge of the Trabucador bar (the only section of the bar included in this analysis), facing SE in the south-western end of zone B (Fig. 9c, segments 33–34 in Fig. 6). In this section the shoreline experienced a maximum retreatment that exceeded 100 m associated to Storm Gloria.

4.3. Recovery process of the Ebro Delta beaches following Storm Gloria

Taking the shoreline position prior to Storm Gloria as a reference, it is possible to quantify the displacements associated with the storm as well as the subsequent recovery throughout the consecutive months.

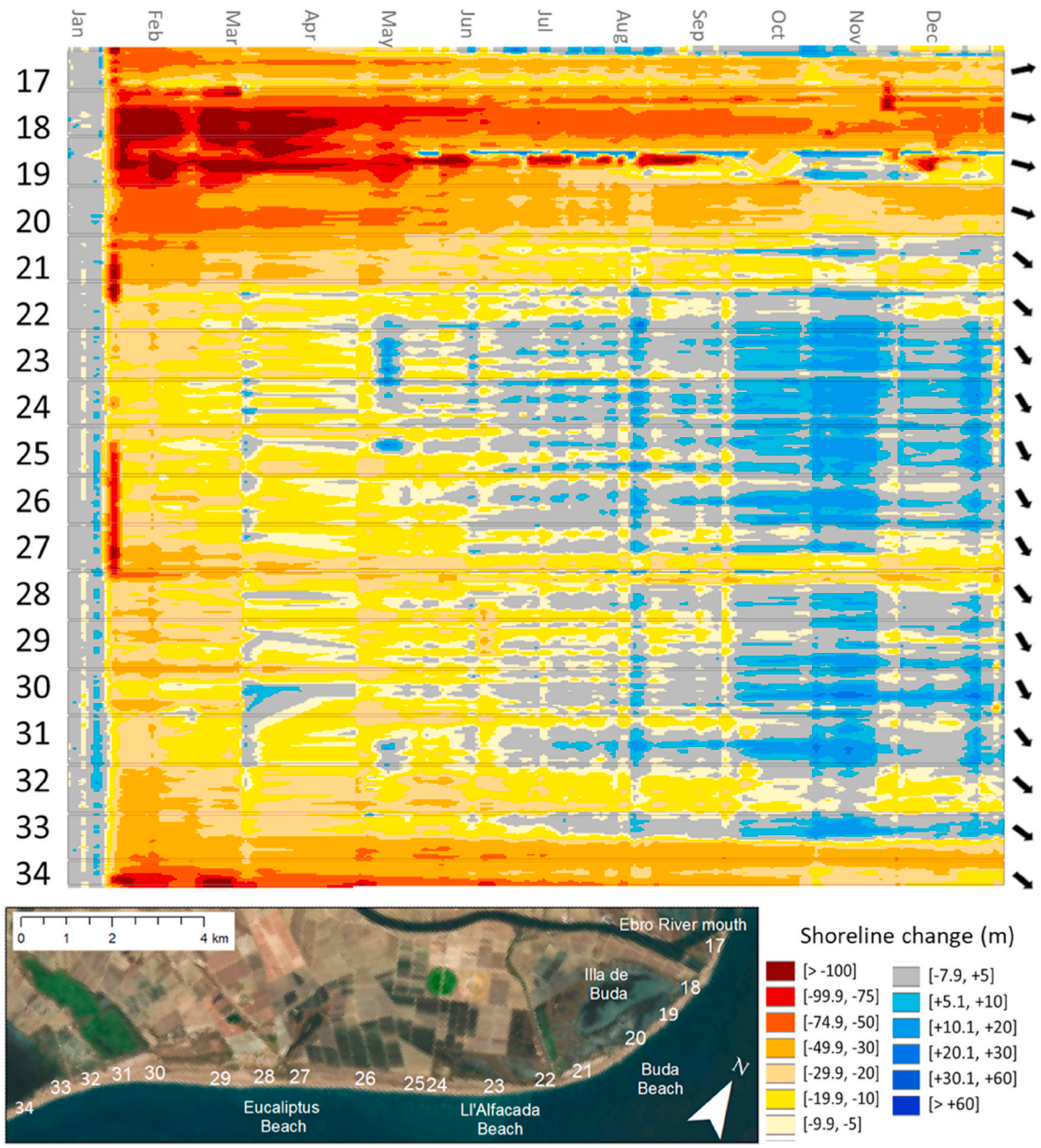

Fig. 6. Shoreline position changes at sector B covering 17 km at the centre of the study area. The locations are presented in the image at the bottom, while the arrows on the right column represent the direction of a cross-shore profile towards the sea.

After the impact of Storm Gloria, a significant and generalised recovery process started along the whole Delta (Table 2) and continued during the following months (Table 3). During the first days after the major retreat the recovery process was very intense (average recovery of 5.44 m per day between the 23 and 26 January), especially in the sector B (7.43 m/d). Progressively during the following weeks, the shoreline position started to stabilize, showing an average retreat of −25 m by mid-February. The recovery process continued more slowly throughout the winter (0.17 m/d), and was reduced along spring (0.10 m/d), being less intense in the sector A than in B and C.

Like the impact, the recovery did not affect the whole Delta homogeneously (Fig. 10). Although the sector B experienced the highest recovery in the short term, the average shoreline position in February shows the remarkable beach loss in certain segments in the easternmost part of the delta (south of the river mouth and northeast of Buda Island). Between end of April and end of August, the accretion of large coastal sections took place, such as along km 9 and 12–14 of sector A, as well as south of km 22 in sector B. Thus, In May there was an average retreat of about 20 m, while the segments with retreats greater than 80 m had already disappeared. However, in the northern and central sectors there was no clear recovery; at least until the end of July, both sectors continued with a loss of about 25 m on average. The recovery trend continued to August (about 10 m of average retreat) when one third of the coastline showed relative stability compared to the location of the shoreline prior to Storm Gloria. From August onwards, however, the recovery was moderated and uneven among the three sectors. The central zone showed a slight recovery that reached its maximum at the end of October when the loss stood at less than 2 m. The northern and southern areas, however, did not show significant recovery during autumn, although there was considerable variability. Among those

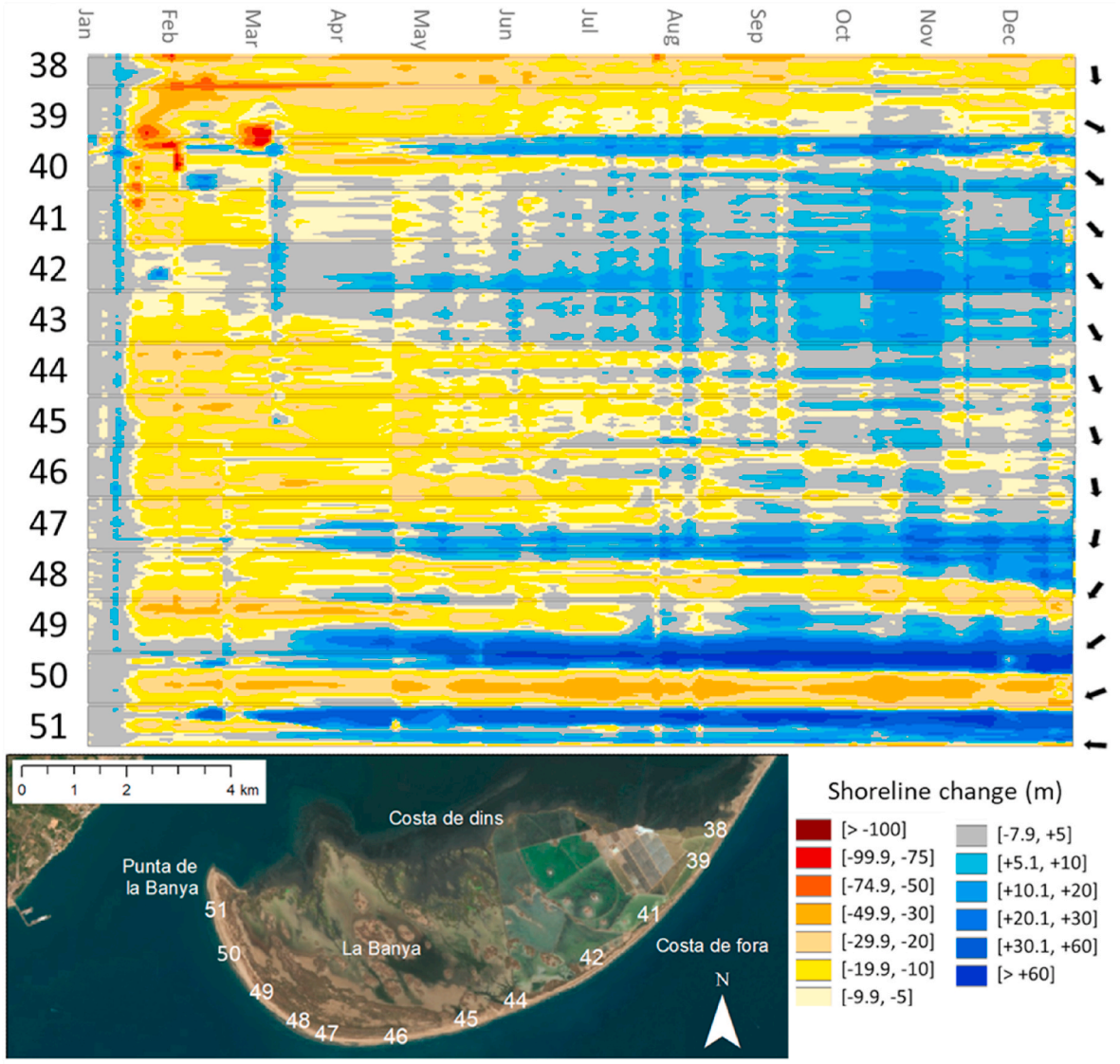

Fig. 7. Shoreline position changes at sector C covering the southernmost 13 km of the study area. The locations are presented in the image at the bottom, while arrows on the right column show the direction of a cross-shore profile towards the sea.

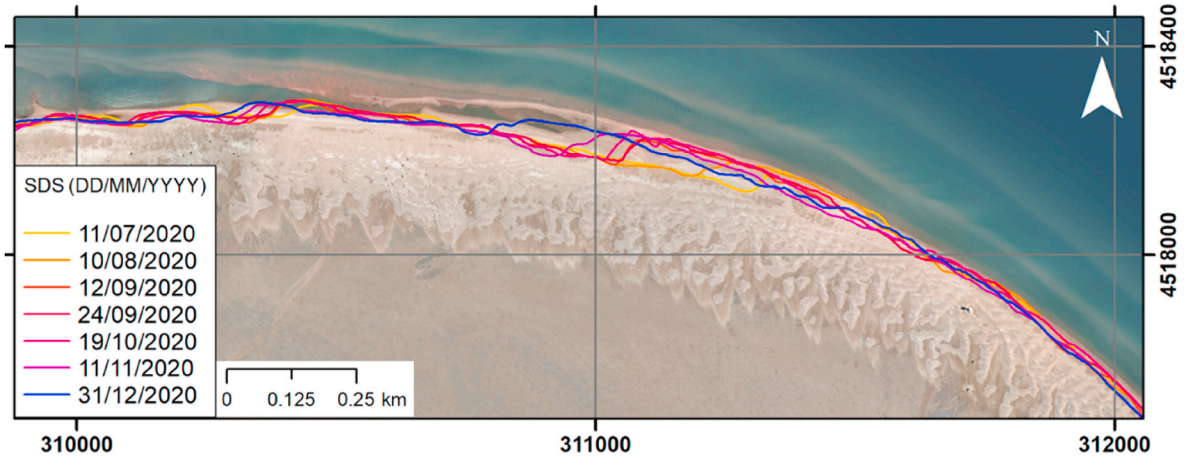

Fig. 8. Detail of the SDSs showing a sandwave moving westwards in sector A (see Fig. 5). Coord. system: ETRS89 UTM31N.

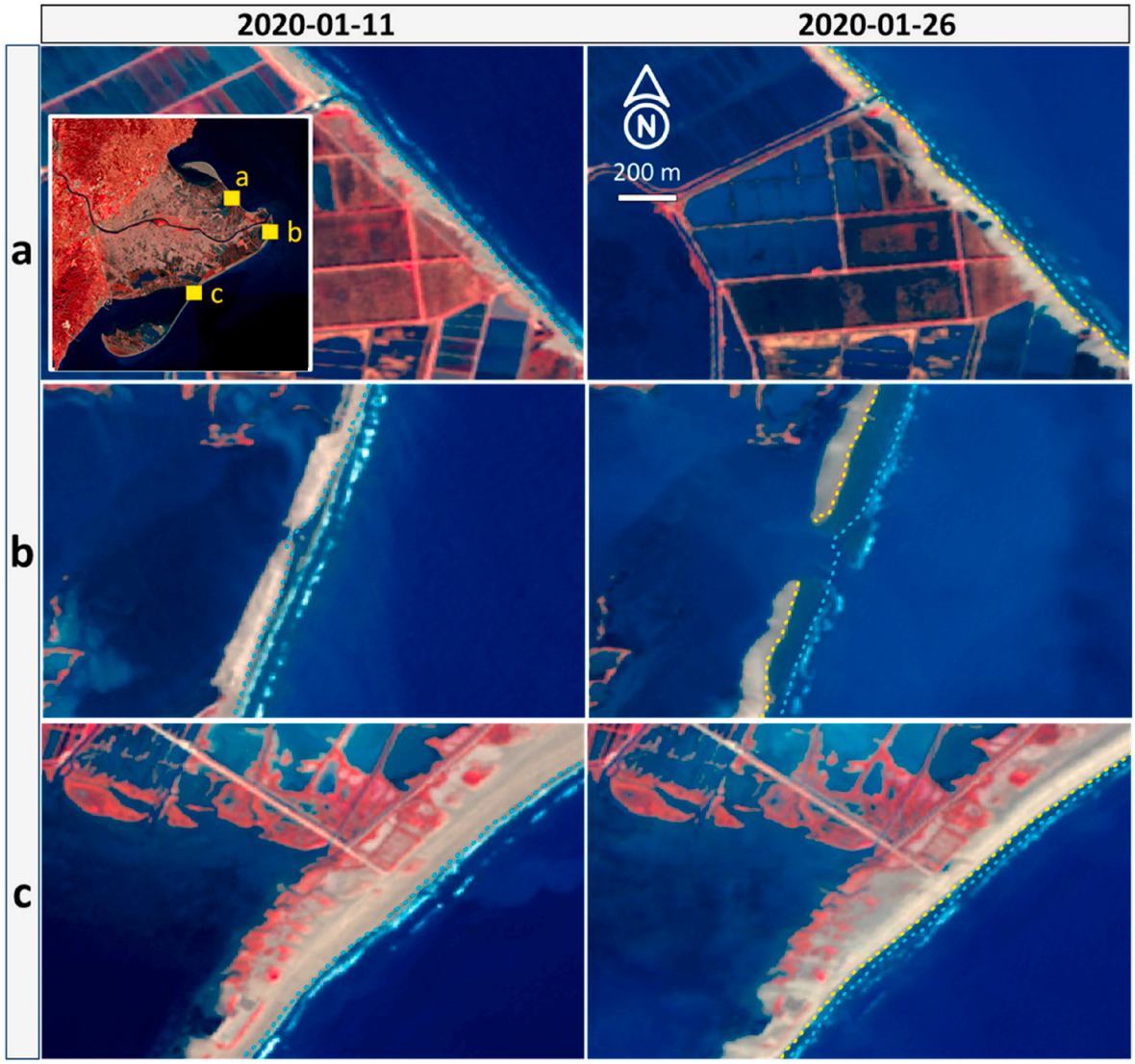

Fig. 9. Examples of shoreline change associated to Storm Gloria in three zones with strong erosion: (a) La Marquesa, (b) Buda Island, and (c) Northern extreme of the Trabucador bar. The SDSs (dashed lines) are superimposed to the false colour infrared composites from the Sentinel-2 images obtained just before (11/01/2020, in blue) and after (26/01/2020, in yellow) the storm episode.

Table 2
Average shoreline changes during different periods after Storm Gloria, expressed as meters per day.

Period	Short-term post storm (3 days)	End of winter	Spring	Summer	Autumn/early winter	Overall post storm
Start-end date (dd/mm)	23/01–26/01	26/01–21/03	21/03–21/06	21/06–22/09	22/09–31/12	23/01–31/12
no. SDSs analysed	2	12	15	28	23	77
Total Delta Rate (m/d)	5.44	0.17	0.10	0.03	−0.03	0.07
Sector A	2.62	0.13	0.11	−0.03	−0.01	0.03
Sector B	7.43	0.23	0.16	0.05	0.05	0.10
Sector C	2.66	0.18	0.18	0.05	−0.04	0.06

changes, the storm the 2 October (wave power = 222 kW/m^{3}s) appeared linked to a generalised recovery (about 3.3 m). Several times the shoreline position showed an inverse response in the diverse sectors. Thus, between the 11 and 16 November there was a strong retreat in the central and southern part, while the northern part remained almost stable. Similarly, associated to the event the 28 November (wave power = 492 kW/m^{3}s) sector C was the only one showing recovery. In December, 41% of the coastline presented total recovery comparing to the situation pre-Storm Gloria (see Table 3), while another 10% presented excess recovery. However, at that time, about 50% of the remaining coastline showed partial recovery, with retreat of more than 10 m when compared to the pre-storm situation.

5. Discussion

Shoreline position constitutes a useful indicator to describe the evolution of a beach and its response to coastal storms. The efficient extraction of SDSs from satellite images that can be accomplished using tools such as SAET (Palomar-Vázquez et al., 2023) offers an opportunity to monitor the impact of disruptive events over the beach morphology and the subsequent recovery. The organisation of the shoreline data into STMs as proposed by Cabezas-Rabadán et al. (2019b) enables the

Table 3
Coastline length of the Ebro Delta (%) experiencing a certain magnitude of shoreline changes during 2020. The average shoreline position in January before Storm Gloria is taken as a reference. Values in bold highlight changes below 5 m (assimilated to a stable situation).

Shoreline change (m)	Feb	Mar	Apr	May	Jun	Jul	Aug	Sep	Oct	Nov	Dec
[>−80]	4.3	4.3	0.0	0.0	0.0	0.0	0.0	0.0	0.0	0.0	0.0
[-79.9, −60]	4.3	0.0	4.3	6.5	21.7	19.6	13.0	4.3	10.9	15.2	15.2
[-59.9, −40]	10.9	2.2	6.5	10.9	6.5	6.5	4.3	4.3	2.2	8.7	4.3
[-39.9, −20]	43.5	28.3	21.7	19.6	19.6	15.2	17.4	17.4	10.9	13.0	15.2
[-19.9, −10]	26.1	41.3	39.1	34.8	19.6	19.6	19.6	19.6	13.0	10.9	13.0
[-9.9, −5]	8.7	15.2	10.9	2.2	0.0	2.2	2.2	2.2	4.3	2.2	0.0
[-4.9, +5]	**2.2**	**8.7**	**15.2**	**21.7**	**26.1**	**30.4**	**32.6**	**37.0**	**32.6**	**28.3**	**41.3**
[+5.1, +10]	0.0	0.0	2.2	2.2	2.2	2.2	6.5	10.9	15.2	13.0	6.5
[+10.1, +20]	0.0	0.0	0.0	2.2	4.3	4.3	2.2	2.2	8.7	6.5	2.2
[>+20]	0.0	8.7	0.0	0.0	0.0	0.0	2.2	2.2	2.2	2.2	2.2

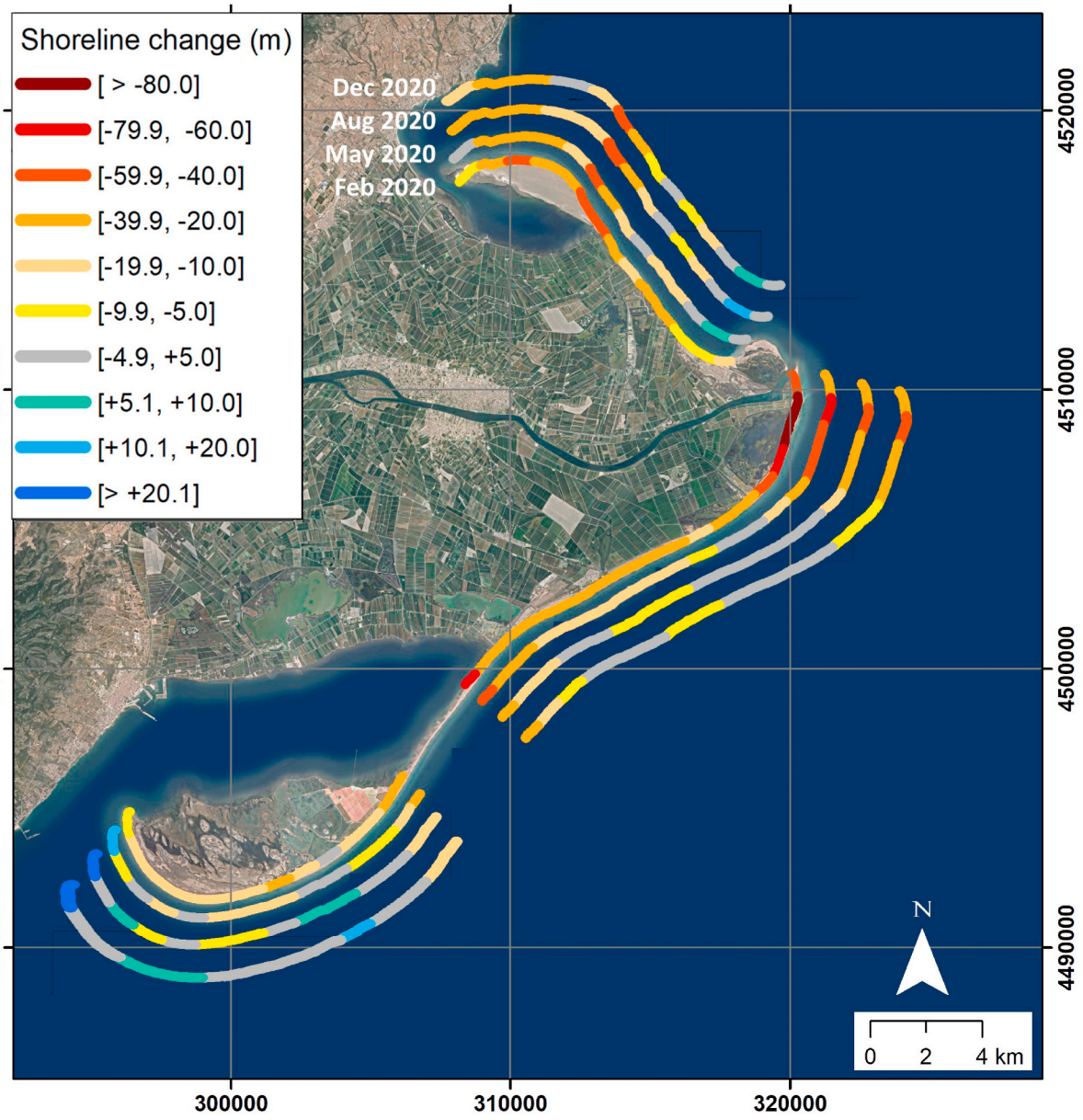

Fig. 10. Shoreline positional changes taking as reference the average position in January 2020 before Storm Gloria. The analysis quantifies the impacts of the storm according to the average position in February, as well as its subsequent recovery until May, August, and December. Coord. system: ETRS89 UTM 31N.

subsequent analysis of shoreline changes at different temporal and spatial scales. Thus, the proposed methodological approach enables studying the behaviour of the beaches composing a complex morphological unit as the Ebro Delta before and after an extreme event such as Storm Gloria.

5.1. Impact and recovery of the Ebro Delta beaches

Accumulative and erosive patterns defined by the shoreline positional changes appear coincidental in time with changing wave conditions. Thus, the wave data recorded throughout the year (Table 1) enable the identification of long periods of calm conditions and episodes of storms. According to that, storms appeared closely associated with generalised changes in the shoreline position throughout the whole delta. Although several storms were registered during 2020, Storm Gloria (the largest event) was the one that conditioned the shoreline position to the greatest extent. This storm clearly marked a turning point for the morphology of the Delta beaches, with an average of 57 m of retreat in the first SDS defined after the storm (23/01/20). Considerable diversity in erosion rates were recorded around the Ebro Delta. Thus, the easternmost section (sector B) experienced the greatest retreat after the storm – with several segments exceeding 100 m (see Figs. 4 and 6), and this was followed by the northern and, to a lesser extent, the southern sections. The changes from this date onwards were much less pronounced, but an erosive situation with respect to the situation before Storm Gloria was maintained almost throughout the whole year.

The orientation of the coast together with the sediment dynamics seem to determine where the greatest shoreline impact occurs and how long it is maintained. This is the case of certain beach segments of that can be identified storm hotspots following Storm Gloria as they experienced extreme erosion maintained over time, without recovering their pre-storm status by the end of the year. Results show that Buda Island, the northern part of sector B, experienced the highest erosive taxes. Buda Island is a sensitive area facing E and located in the easternmost part of the Delta, therefore especially exposed to storms. In this section the bar breached resulted in the inundation of the inner lagoon (see Fig. 9), a phenomenon that has already been reported in different occasions in the past (Jiménez et al., 2012). This section experienced a remarkably slow recovery, mainly showing above 100 m retreat in mid-April and in different episodes during autumn. By the end of the year the recovery was only partial (retreat ranging from 10 to 20 m), which is in line with the annual rates estimated during the last decades (Valdemoro et al., 2007). Buda presents a limited capacity for recovery since it receives no external supplies of sand as sediment inputs from the river are currently extremely scarce (Jiménez and Sánchez-Arcilla, 1993). Another of the identified hotspots is Marquesa Beach (central part of sector A, NE-facing) probably due to its almost perpendicular orientation with respect to the waves during Gloria (as well as most of the storms that occurred in the site). This translated into severe overwash flooding during Storm Gloria (see Fig. 9, also reported by Blay and Àvila, 2020). La Marquesa is a zone previously identified due to high erosion rates and repeated episodes of overwash and flooding (e.g., Aranda et al., 2022; Jiménez et al., 2012). Marquesa presents a limited capacity to accumulate sediment from the surrounding beaches. By the end of the year most of the zone had experienced a partial recovery, but still maintaining a retreat about 10–20 m (30 m in some points), clearly exceeding the 5 m/y estimated by Lavoie et al. (2014) during the 1957–2007. The third hot spot appears in the northern edge of the Trabucador bar, a very low beach segment that was completely overtopped by waves during and after the storm (Berdalet et al., 2020). Breaching have been repeatedly reported over time in the central section of Trabucador linked to the low elevation and narrowness of this unit (e.g., Jiménez et al., 2012; Sánchez-Arcilla and Jiménez, 1994). The shoreline retreated more than 100 m after Storm Gloria, and the displacement was maintained with this magnitude at least until March. Subsequently, the recovery was progressively taken place towards the south, but it was only partial by the end of the year. This annual retreat (10–50 m in the different segments) was far larger than the erosion rates estimated by Jiménez et al. (2012) for the north of the Trabucador during the stormy period 2000–2004 (more than 8 m/y). The three sites with the maximum shoreline retreat during the storm were characterised by a strong overwash (including sandbar breaching at the Buda and N Trabucador sites) and subaerial washover deposits at La Marquesa beach (Fig. 9). Thus, the flooding and overwash processes may have displaced important quantities of sediment landward. Although remaining in the beach system, the availability of sediment for the recovery of the shoreline position is limited. Similar to other measures taken in the past (Blay and Àvila, 2020), emergency actions were taken – consisting of sand mobilisations to rebuild the beach barrier and prevent flooding – and these actions probably favoured the recovery of the coastline in these sectors during the months of February and March. However, the relative relevance of the actions carried out on the beachface for the recovery of the beach is so far unknown.

Shoreline changes show how calm periods appear as a main factor contributing to beach recovery. A quantification of the displacements after Storm Gloria was made to map in detail the impact and the recovery over the subsequent months (see Fig. 10). The most significant recovery occurred in low wave conditions the first days after the peak of the storm. The recovery was fast, with an average rate of 5.44 m/day, reaching 7.43 m/d in the most affected sector B (see Tables 2 and 3), probably as a consequence of a partial recovery of the three-dimensional morphology of the beach. Afterwards, the recovery was progressively reduced, although it continued associated with a long four-month episode of calm waves between the end of April and the end of August. During this period the significant wave heights did not exceed 2 m, confirming a general coincidence between incident wave energy and recovery (Wright and Short, 1984). This pattern of recovery rates is in line with the observations by Phillips et al. (2017) suggesting that, after a first phase in which the sediment is detached from the beachface, the accumulation and fast berm progradation occur followed by slow rates in more advanced recovery stages. Nevertheless, this process does not take place homogeneously. While sectors A and B generally showed similar changes, sector B (more affected by the storm) showed a recovery pattern that was sustained during the year. In certain segments, the lack of recovery could be caused by a combination of cross-shore losses of sediment from the active beach (overwash or to deeper areas) together with an insufficient supply of sediment. From then until the end of the year several episodes of higher waves occurred, and the shoreline experienced an oscillatory pattern and a slightly negative trend in sectors A and C, and positive in sector B. The interruption of the recovery process led to a situation of partial recovery by the end of 2020 as about half of the delta still presented a significant retreat. This partial recovery is a common phenomenon after extreme storms as beaches may need more than one summer season or even years to recover (e.g., Castelle et al., 2015). With this in mind, a longer series of SDSs would be needed to be able to analyse in the medium-long term the consequences of Storm Gloria in the Ebro Delta beaches and to determine if a complete recovery is achieved.

The characterisation of the shoreline changes after Storm Gloria supports the idea that following a storm the beach response is greatly dependent on the orientation of the beach with respect to the waves (Burvingt et al., 2017), and the higher vulnerability of beach-barrier systems. In these circumstances, cross-shore sediment losses and longshore sediment transport gradients are both relevant. On the contrary, during medium-sized storms there is no sediment loss from the beach system, and the recovery of the shoreline position mainly depends on longitudinal sediment transport gradients together with the potential return of sediment to the beach from deeper areas. In line with that and regarding the identified hotspots in the Ebro Delta, it can be seen how Marquesa Beach presents an almost perpendicular orientation to the waves during Storm Gloria. At the same time, Buda Island and the northern part of the Trabucador Bar constitute very sensitive

beach-barrier systems. Finally, longshore sediment transport gradients favour the accumulation of sediment at the end of the spits, contributing to the formation of mesoforms as the identified sandwaves (see Fig. 9).

At this point, it is important to highlight the role of the storms in the shoreline recovery. Several storms smaller than Gloria do not appear linked to clear shoreline retreat and, on the contrary, they even appear associated with accretion in certain sectors. The consecutive storms that occurred during spring appear to be related to the start of an accumulative behaviour in several segments, while on certain occasions, the shoreline position shows an inverse response in the diverse sectors (see Fig. 4). Depending on the previous morphological state of the beach and the direction of the storm those events can contribute to the recovery by mobilising sediment from the bar and increasing the volume of available sand on the subaerial beach. These displacements of sand were previously pointed out by different authors as an essential recovery mechanism, and it supports the idea that recovery does not necessarily occur during calm periods being energetic events essential for the mobilisation of the sediment (Scott et al., 2016), although this is not observed in our data.

5.2. Advantages and constraints of the methodology and future research

An analysis of the STMs enables us to recognise the dynamic processes that take place at different spatial and temporal scales in the studied area. When considering the Ebro Delta as a unit, it is evident that the differentiation of three sectors is insufficiently detailed to capture the evolutionary dynamics of such a complex area. To overcome this issue, it is possible to zoom into the STMs to identify small-scale evolutionary processes. The accuracy provided by the sub-pixel SDSs facilitates analysis at a greater scale of detail and the identification of mesoscale forms such as the movement of a sandwave (Fig. 8), or the elongation of sand spits at the northern and southern ends of the study area (Figs. 5 and 7).

There are periods with almost no data. Thus, a notable data gap appears between mid-March and the end of April (5 and 4 SDSs for those months respectively) due to an abnormally long period of cloudiness after the stormy season at the end of winter. In these periods, the interpolation leading to the STMs is compromised and results must be interpreted carefully. Given that recovery in microtidal beaches can take place within a few days (Ranasinghe et al., 2012), it is possible that retreat and recovery after storms occurred during periods when no data are available, making adequate detection impossible. However, despite the gap in source data satellite imagery, there is a high level of coverage throughout the year (93 images, that is one shoreline position every four days). This enables the evolutionary sequence to be mapped continuously and with a frequency far greater than that usually obtained from DGPS and UAVs that require in situ work. Furthermore, the current availability of Landsat 9 satellite images (which can also be used by SAET for extracting SDSs) establishes a new scenario with more data available.

The accuracy of the shoreline positions ranges from 2.62 m to 8.67 m RMSE for the Western Mediterranean (Palomar-Vázquez et al., 2023; Pardo-Pascual et al., 2023), which appears in line with the those provided by other shoreline extraction tools for microtidal environments (Vos et al., 2023). Although the errors associated with the method can introduce noise in the time series obtained, the main trends are captured. The magnitudes of shoreline change associated with extreme storms are far larger than the accuracy level of the technique validating its use for monitoring purposes. Furthermore, the correction of the STMs carried out in this work according to the tide and wave set-up helps distinguish the variability in shoreline position changes caused by morphological variability from those originated by water level changes, which is a key issue for correctly interpreting the information provided by the SDSs (Castelle et al., 2021; Konstantinou et al., 2023). In the present work, the accuracy of the horizontal shifting carried out has been hampered by the time lag between the available slope data and the shoreline extraction and the employment of a single value. The high variability in beach slope (between +1 and −1 m) in response to wave conditions is well known, but unfortunately, there are no topographic measurements coincident in time with the series of satellite images. The horizontal correction could be improved using spatial and timely variant slope data, which could potentially be obtained from topographic profiles or satellite images (Vos et al., 2020).

In certain coastal sections, shoreline extraction cannot be properly carried out given the complex form and structure of the beach. This is the case of El Trabucador bar (narrower than 100 m at certain points), and the river mouth in which the narrowness and the intermittent presence of shallow sand banks impeded obtaining reliable shoreline data. The analysis of this type of coastal segment may be possible with shoreline extraction techniques adapted to the particularities of each area (e.g., Angelats et al., 2022; Cabezas-Rabadán et al., 2020; Konstantinou et al., 2023; Pardo-Pascual et al., 2023), but not with the methodology used in this work to homogeneously analyse the entire delta.

Considering the critical situation of the Ebro Delta beaches, it is important to provide managers with up-to-date information to ensure optimal decision making. The integration of an automatic shoreline extraction tool such as SAET with analysis tools such as the STMs brings a direct application of satellite images for coastal management. To obtain a holistic view of the sedimentary situation of the affected beaches, data provided by SDSs and STMs may be complemented with three-dimensional data of the dunes and emerged beach (e.g., Calleja-Cascajero and Rodríguez-Santalla, 2021; Pardo-Pascual et al., 2021) and bathymetry (e.g., Viaña-Borja et al., 2023).

6. Conclusions

Using the SAET extraction tool and the freely available S2 and L8 images enables efficiently and accurately defining the shoreline changes caused by major storms at a regional scale. The analysis of STMs in conjunction with wave data has enabled mapping the shoreline positional shifts and quantifying the impact and recovery processes that follow coastal storms. The results evidence the enormous importance for the medium-term evolution of beaches of the highly energetic storms that cause erosive hotspots. A large storm such as Gloria appears as a disruptive event that constitutes a shifting point in the shoreline trends. After these storms, recovery is slow with differing intensities along the coast, and recovery mainly occurs when low-energetic episodes persist. The analysis of the shoreline changes evidences the role of calm wave periods in beach recovery, with a response that varies along the coast and is apparently related to orientation and local sediment transport patterns. Shoreline recovery was faster in the immediate aftermath of the storm and slowed over the following months. One year after the extreme storm, approximately 50% of the coastline had recovered its pre-storm shoreline position, although sand mobilisation actions in certain sectors may have promoted this recovery to an unquantified extent.

The exploitation of the shorelines largely depends on the accuracy and frequency of data acquisition, something in which the methodology presented in this work stands out from other techniques. The SAET tool implements the necessary workflow to provide relatively simple and comprehensive sets of updated shorelines for long coastal stretches. Moreover, the efficient management of the obtained SDSs, and their organisation in STMs of the shoreline changes, provides the holistic and homogeneous approach required for coastal monitoring systems.

CRediT authorship contribution statement

C. Cabezas-Rabadán: Conceptualization, Data curation, Formal analysis, Funding acquisition, Investigation, Methodology, Project administration, Software, Supervision, Visualization, Writing – original draft, Writing – review & editing. **J.E. Pardo-Pascual:**

Conceptualization, Data curation, Formal analysis, Funding acquisition, Investigation, Methodology, Project administration, Software, Supervision, Visualization, Writing – review & editing. **J. Palomar-Vázquez:** Conceptualization, Data curation, Investigation, Methodology, Software, Visualization, Writing – review & editing. **A. Roch-Talens:** Visualization, Writing – review & editing. **J. Guillén:** Conceptualization, Formal analysis, Funding acquisition, Investigation, Project administration, Supervision, Visualization, Writing – review & editing, Writing – original draft.

Declaration of competing interest

The authors declare that they have no known competing financial interests or personal relationships that could have appeared to influence the work reported in this paper.

Data availability

As presented in the methods section, available free of charge from the Copernicus Open Access Hub and the Earth Explorer of the U.S. Geological Survey (USGS).

Acknowledgements

The ECFAS (European Coastal Flood Awareness System) project (https://www.ecfas.eu/) has received funding from the EU H2020 research and innovation programme under grant agreement No. 101004211. This research is also supported by the projects MONOBESAT (PID2019-111435RB-I00) funded by the Spanish Ministry of Science, Innovation and Universities, the M. Salas contract (Re-qualification programme) by the Ministry of Universities financed by the EU – NextGenerationEU and Primeros Proyectos de Investigación (PAID-06-22) by Vicerrectorado de Investigación de la Universitat Politècnica de València (UPV). J. Guillén's work is supported by the MOLLY project (PID2021-124272OB-C21) and 'Severo Ochoa Centre of Excellence' accreditation (CEX2019-000928-S) funded by AEI 10.13039/501100011033. Authors acknowledge USGS and ESA for providing free access to the Sentinel-2 and Landsat imagery, and Puertos del Estado for the oceanographic data, and the reviewers for their insightful feedback.

References

Almeida, L.P., de Oliveira, I.E., Lyra, R., Dazzi, R.L.S., Martins, V.G., da Fontoura Klein, A.H., 2021. Coastal analyst system from space imagery engine (CASSIE): shoreline management module. Environ. Model. Software 140, 105033.

Amarouche, K., Bingölbali, B., Akpinar, A., 2021. New wind-wave climate records in the western mediterranean sea. Clim. Dynam. 1–24.

Amores, A., Marcos, M., Carrió, D.S., Gómez-Pujol, L., 2020. Coastal impacts of storm Gloria (January 2020) over the north-western mediterranean. Nat. Hazards Earth Syst. Sci. 20 (7), 1955–1968.

Anfuso, G., Loureiro, C., Taaouati, M., Smyth, T., Jackson, D., 2020. Spatial variability of beach impact from post-tropical cyclone Katia (2011) on northern Ireland's north coast. Water 12 (5), 1380. https://doi.org/10.3390/w12051380.

Angelats, E., Soriano-González, J., Puig i Polo, C., Guillén-Aranda, J., Falqués Serra, A., Ribas Prats, F., 2022. Monitoring coastal storms' effects on the Trabucador barrier beach (Ebro Delta) through Sentinel-2 derived shorelines. XI Jornadas de Geomorfología Litoral: Galicia 2022: Santiago de Compostela 27–29, 1–4 de julio de 2022: actas.

Aranda, M., Gracia, F.J., Rodríguez-Santalla, I., 2022. Historical Morphological Changes (1956-2017) and Future Trends at the Mouth of the Ebro River Delta (NE Spain).

Ariza, E., Jiménez, J.A., Srdá, R., 2008. A critical assessment of beach management on the Catalan coast. Ocean Coast Manag. 51 (2), 141–160.

Berdalet, E., Marrasé, C., Pelegrí, J.L., 2020. Resumen sobre la Formación y Consecuencias de la Borrasca Gloria (19-24 enero 2020). (ICM) Informes y documentos de trabajo, p. 38. https://doi.org/10.20350/digitalCSIC/12496.

Bishop-Taylor, R., Sagar, S., Lymburner, L., Alam, I., Sixsmith, J., 2019. Sub-pixel waterline extraction: characterising accuracy and sensitivity to indices and spectra. Rem. Sens. 11 (24), 2984.

Blay, J., Àvila, A., 2020. Els efectes del temporal Glòria: una mostra de la necessitat d'actuació urgent al delta de l'Ebre. Treballs de la Societat Catalana de Geografia, pp. 163–189.

Boak, E.H., Turner, I.L., 2005. Shoreline definition and detection: a review. J. Coast Res. 21 (4), 688–703.

Burvingt, O., Masselink, G., Russell, P., Scott, T., 2017. Classification of beach response to extreme storms. Geomorphology 295, 722–737.

Cabezas-Rabadán, C., Pardo-Pascual, J.E., Almonacid-Caballer, J., Rodilla, M., 2019a. Detecting problematic beach widths for the recreational function along the Gulf of Valencia (Spain) from Landsat 8 subpixel shorelines. Appl. Geogr. 110, 102047.

Cabezas-Rabadán, C., Pardo-Pascual, J.E., Palomar-Vázquez, J., 2021. Characterizing the relationship between the sediment grain size and the shoreline variability defined from sentinel-2 derived shorelines. Rem. Sens. 13 (14), 2829.

Cabezas-Rabadán, C., Pardo-Pascual, J.E., Palomar-Vázquez, J., Fernández-Sarría, A., 2019b. Characterizing beach changes using high-frequency Sentinel-2 derived shorelines on the Valencian coast (Spanish Mediterranean). Sci. Total Environ. 691, 216–231.

Cabezas-Rabadán, C., Pardo-Pascual, J.E., Palomar-Vázquez, J., Ferreira, O., Costas, S., 2020. Satellite derived shorelines at an exposed meso-tidal beach. J. Coast Res. 95 (SI), 1027–1031.

Calleja-Cascajero, D., Rodríguez-Santalla, I., 2021. Volumetric change of the coastal dunes of the Isla de Buda (Ebro delta) between 2005 and 2017 using LIDAR data. Environ. Sci. Proc.

Castelle, B., Harley, M., 2020. Extreme events: impact and recovery. In: Sandy Beach Morphodynamics. Elsevier, pp. 533–556.

Castelle, B., Masselink, G., Scott, T., Stokes, C., Konstantinou, A., Marieu, V., Bujan, S., 2021. Satellite-derived shoreline detection at a high-energy meso-macrotidal beach. Geomorphology 383, 107707.

Castelle, B., Marieu, V., Bujan, S., Splinter, K.D., Robinet, A., Sénéchal, N., Ferreira, S., 2015. Impact of the winter 2013-2014 series of severe Western Europe storms on a double-barred sandy coast: beach and dune erosion and megacusp embayments. Geomorphology 238, 135–148.

Ciavola, P., Coco, G. (Eds.), 2017. Coastal Storms: Processes and Impacts. John Wiley Sons.

de Alfonso, M., Lin-Ye, J., García-Valdecasas, J.M., Pérez-Rubio, S., Luna, M.Y., Santos-Muñoz, D., et al., 2021. Storm Gloria: sea state evolution based on in situ measurements and modeled data and its impact on extreme values. Front. Mar. Sci. 8, 646873.

Flor-Tey, G., 2021. Anàlisi dels impactes sobre la costa del Mediterrani Occidental provocats per la Tempesta Glòria (Master's thesis. Universitat Politècnica de Catalunya.

Guillén, J., 2020. Impacto sobre la franja litoral: Introducción. Vulnerabilidad en la costa catalana: ejemplos de dinámica litoral. Salidas y entradas de sedimentos en la playa.

Guillén, J., Palanques, A., 1993. Longshore bar and trough systems in a microtidal, storm-wave dominated coast: the Ebro Delta (NW Mediterranean). Mar. Geol. 115, 239–252.

Hagenaars, G., de Vries, S., Luijendijk, A.P., de Boer, W.P., Reniers, A.J., 2018. On the accuracy of automated shoreline detection derived from satellite imagery: a case study of the sand motor mega-scale nourishment. Coast. Eng. 133, 113–125.

Hu, P., Li, Z., Zeng, C., Zhu, D., Liu, R., Su, Q., Tang, J., Zhu, Y., 2023. Bed level changes in the surf zone during post-storm beach recovery. Front. Mar. Sci. 10, 1233068 https://doi.org/10.3389/fmars.2023.1233068.

IPCC, 2021. Summary for policymakers. In: Zhai, P., Pirani, A., Connors, S.L., Péan, C., Berger, S., Caud, N., Chen, Y., Goldfarb, L., Gomis, M.I., Huang, M., Leitzell, K., Lonnoy, E., Matthews, J.B.R., Maycock, T.K., Waterfield, T., Yelekçi, O., Yu, R., Zhou, B. (Eds.), Climate Change 2021: the Physical Science Basis. Contribution of Working Group I to the Sixth Assessment Report of the Intergovernmental Panel on Climate Change [Masson-Delmotte, V. Cambridge University Press, Cambridge, United Kingdom and New York, NY, USA, pp. 3–32.

Jiménez, J.A., Sánchez-Arcilla, A., 1993. Medium-term coastal response at the Ebro delta, Spain. Mar. Geol. 114 (1–2), 105–118.

Jiménez, J.A., Sancho-García, A., Bosom, E., Valdemoro, H.I., Guillén, J., 2012. Storm-induced damages along the Catalan coast (NW Mediterranean) during the period 1958–2008. Geomorphology 143, 24–33.

Jiménez, J., Sánchez-Arcilla, A., Valdemoro, H.I., Gracia, V., Nieto, F., 1997. Processes reshaping the Ebro delta. Mar. Geol. 144 (1–3), 59–79.

Konstantinou, A., Scott, T., Masselink, G., Stokes, K., Conley, D., Castelle, B., 2023. Satellite-based shoreline detection along high-energy macrotidal coasts and influence of beach state. Mar. Geol., 107082

Lavoie, C., Jiménez, J.A., Canals, M., Lastras, G., De Mol, B., Amblas, D., et al., 2014. Influence on present-day coastal dynamics and evolution of a relict subaqueous delta lobe: Sol de Riu lobe, Ebro Delta. Continent. Shelf Res. 74, 94–104.

Lee, G.H., Nicholls, R.J., Birkemeier, W.A., 1998. Storm-driven variability of the beach-nearshore profile at Duck, North Carolina, USA, 1981–1991. Mar. Geol. 148 (3–4), 163–177.

List, J.H., Farris, A.S., Sullivan, C., 2006. Reversing storm hotspots on sandy beaches: spatial and temporal characteristics. Mar. Geol. 226 (3–4), 261–279.

Liu, Q., Trinder, J., Turner, I.L., 2017. Automatic super-resolution shoreline change monitoring using Landsat archival data: a case study at Narrabeen–Collaroy Beach, Australia. J. Appl. Remote Sens. 11 (1), 016036-016036.

Morton, R.A., Paine, J.G., Gibeaut, J.C., 1994. Stages and durations of post-storm beach recovery, southeastern Texas coast, USA. J. Coast Res. 884–908.

Palomar-Vázquez, Pardo-Pascual, Almonacid-Caballer, Cabezas-Rabadán, 2023. Shoreline Analysis and Extraction Tool (SAET): a new tool for the automatic extraction of satellite-derived shorelines with subpixel accuracy. Rem. Sens. 15 (12), 3198. https://doi.org/10.3390/rs15123198.

Pardo-Pascual, J.E., Almonacid-Caballer, J., Ruiz, L.A., Palomar-Vázquez, J., 2012. Automatic extraction of shorelines from Landsat TM and ETM+ multi-temporal images with subpixel precision. Rem. Sens. Environ. 123, 1–11.

Pardo-Pascual, J.E., Almonacid-Caballer, J., Ruiz, L.A., Palomar-Vázquez, J., Rodrigo-Alemany, R., 2014. Evaluation of storm impact on sandy beaches of the Gulf of Valencia using Landsat imagery series. Geomorphology 214, 388–401.

Pardo-Pascual, J.E., Cabezas-Rabadán, C., Palomar-Vázquez, J., 2021. Anàlisi dels canvis morfològics del cordó dunar i les platges de la Devesa del Saler a conseqüència del temporal Gloria. In: Rosselló, A. Vicenç M., geògraf (Eds.), Als Seus 90 Anys, vol. 30. Publicacions de la Universitat de València, pp. 393–418, 978-84-9133-428-6.

Pardo-Pascual, J.E., Palomar-Vázquez, J.M., Cabezas-Rabadán, C., 2022a. Analysis of the morphological changes of the beaches along the segment València-Cullera (E Spain) from satellite-derived shorelines. Cuadernos de Investigación Geográfica 48 (2), 309–324.

Pardo-Pascual, J.E., Palomar-Vázquez, J., Cabezas-Rabadán, C., 2022b. Estudio de los cambios de posición de la línea de costa en las playas del segmento València-Cullera (1984-2020) a partir de imágenes de satélite de resolución media de libre acceso. Cuadernos de Geografía de la Universitat de València, pp. 79–104, 108-9.

Pardo-Pascual, J.E., Almonacid-Caballer, J., Cabezas-Rabadán, C., Fernández-Sarría, A., Armaroli, C., Ciavola, P., Montes, J., Souto-Ceccon, P.E., Palomar-Vázquez, J., 2023. Assessment of Satellite-Derived Shorelines Automatically Extracted from Sentinel-2 Imagery Using SAET. Coastal Engineering. https://doi.org/10.1016/j.coastaleng.2023.104426. ISSN 0378-3839.

Pérez-Gómez, B., García-León, M., García-Valdecasas, J., Clementi, E., Mösso Aranda, C., Pérez-Rubio, S., et al., 2021. Understanding sea level processes during Western Mediterranean storm Gloria. Front. Mar. Sci. 8, 647437.

Phillips, M.S., Blenkinsopp, C.E., Splinter, K.D., Harley, M.D., Turner, I.L., 2019. Modes of berm and beachface recovery following storm reset: observations using a continuously scanning lidar. J. Geophys. Res.: Earth Surf. 124, 720–736. https://doi.org/10.1029/2018JF004895.

Phillips, M.S., Harley, M.D., Turner, I.L., Splinter, K.D., Cox, R.J., 2017. Shoreline recovery on wave-dominated sandy coastlines: the role of sandbar morphodynamics and nearshore wave parameters. Mar. Geol. 385, 146–159.

Pintó, J., Garcia-Lozano, C., Sardá, R., Roig-Munar, F.X., Martí, C., 2020. Efectes del temporal Glòria sobre el litoral. Treballs de la Societat Catalana de Geografia, pp. 89–109.

Prodger, S., Russell, P., Davidson, M., Miles, J., Scott, T., 2016. Understanding and predicting the temporal variability of sediment grain size characteristics on high-energy beaches. Mar. Geol. 376, 109–117.

Ranasinghe, R., Holman, R., De Schipper, M.A., Lippmann, T., Wehof, J., Duong, T.M., et al., 2012. Quantifying nearshore morphological recovery time scales using argus video imaging: Palm Beach, Sydney and Duck, North Carolina. In: ICCE 2012: Proceedings of the 33rd International Conference on Coastal Engineering. Coastal Engineering Research Council, Santander, Spain, pp. 1–6. July 2012.

Rodríguez-Santalla, I., Somoza, L., 2019. The Ebro River delta. The Spanish coastal systems: dynamic processes. Sedim. Manag. 467–488.

Sánchez-Arcilla, A., Jiménez, J.A., 1994. Breaching in a wave-dominated barrier spit: the trabucador bar (north-eastern Spanish coast). Earth Surf. Process. Landforms 19 (6), 483–498.

Sánchez-García, E., Palomar-Vázquez, J.M., Pardo-Pascual, J.E., Almonacid-Caballer, J., Cabezas-Rabadán, C., Gómez-Pujol, L., 2020. An efficient protocol for accurate and massive shoreline definition from mid-resolution satellite imagery. Coast. Eng. 160, 103732.

Sancho-García, A., Guillén, J., Gracia, V., Rodríguez-Gómez, A.C., Rubio-Nicolás, B., 2021. The use of news information published in newspapers to estimate the impact of coastal storms at a regional scale. J. Mar. Sci. Eng. 9, 497. https://doi.org/10.3390/jmse9050497.

Schlacher, T.A., Schoeman, D.S., Dugan, J., Lastra, M., Jones, A., Scapini, F., McLachlan, A., 2008. Sandy beach ecosystems: key features, sampling issues, management challenges and climate change impacts. Mar. Ecol. 29, 70–90.

Scott, T., Masselink, G., O'Hare, T., Saulter, A., Poate, T., Russell, P., et al., 2016. The extreme 2013/2014 winter storms: beach recovery along the southwest coast of England. Mar. Geol. 382, 224–241.

Sénéchal, N., Castelle, B., Bryan K, R., 2017. Storm clustering and beach response. Coastal storms: Process. Impacts 151–174.

Sénéchal, N., Coco, G., Castelle, B., Marieu, V., 2015. Storm impact on the seasonal shoreline dynamics of a meso-to macrotidal open sandy beach (Biscarrosse, France). Geomorphology 228, 448–461.

Slott, J.M., Murray, A.B., Ashton, A.D., Crowley, T.J., 2006. Coastline responses to changing storm patterns. Geophys. Res. Lett. 33, L18404.

Splinter, K.D., Carley, J.T., Golshani, A., Tomlinson, R., 2014. A relationship to describe the cumulative impact of storm clusters on beach erosion. Coast. Eng. 83, 49–55.

Stockdon, H.F., Holman, R.A., Howd, P.A., Sallenger Jr., A.H., 2006. Empirical parameterization of setup, swash, and runup. Coast. Eng. 53 (7), 573–588.

Valdemoro, H.I., Sánchez-Arcilla, A., Jiménez, J.A., 2007. Coastal dynamics and wetlands stability. The Ebro delta case. Hydrobiologia 577, 17–29.

Viaña-Borja, S.P., Fernández-Mora, A., Stumpf, R.P., Navarro, G., Caballero, I., 2023. Semi-automated bathymetry using Sentinel-2 for coastal monitoring in the Western Mediterranean. Int. J. Appl. Earth Obs. Geoinf. 120, 103328.

Vos, K., Harley, M.D., Splinter, K.D., Walker, A., Turner, I.L., 2020. Beach slopes from satellite-derived shorelines. Geophys. Res. Lett. 47 (14), e2020GL088365.

Vos, K., Splinter, K.D., Harley, M.D., Simmons, J.A., Turner, I.L., 2019. CoastSat: a Google Earth Engine-enabled Python toolkit to extract shorelines from publicly available satellite imagery. Environ. Model. Software 122, 104528.

Vos, K., Splinter, K.D., Palomar-Vázquez, J., Pardo-Pascual, J.E., Almonacid-Caballer, J., Cabezas-Rabadán, C., et al., 2023. Benchmarking satellite-derived shoreline mapping algorithms. Commun. Earth Environ. 4 (1), 345.

Wright, L.D., Short, A.D., 1984. Morphodynamic variability of surf zones and beaches: a synthesis. Mar. Geol. 56, 93–118.